Catalysis Today 148 (2009) 160–168

Contents lists available at ScienceDirect

Catalysis Today

journal homepage: www.elsevier.com/locate/cattod

Study of the *Keggin* structure and catalytic properties of Pt-promoted heteropoly compound/Al-MCM-41 hybrid catalysts

X.K. Yang [a], L.F. Chen [b,*], J.A. Wang [b], L.E. Noreña [c], O. Novaro [d]

[a] School of Chemistry and Chemical Engineering, Xinyang Normal University, Xingyang, 464000, PR China
[b] ESIQIE, Instituto Politécnico Nacional, Col. Zacatenco, 07738 México, D.F., Mexico
[c] Departamento de Ciencias Básicas, Universidad Autónoma Metropolitana-A, Av. San Pablo 180, Col. Reynosa-Tamaulipas, 02200 México, D.F., Mexico
[d] Instituto de Física, Universidad Nacional Autónoma de México, A. P. 20-364, 01000 México, D.F., Mexico

ARTICLE INFO

Article history:
Available online 29 April 2009

Keywords:
Hydroisomerization
n-Heptane
12-Tungstophosphoric acid
Acidity
Catalyst
Al-MCM-4

ABSTRACT

Aluminum-containing mesoporous molecular sieves (referred as WSA*n*, where *n* = Si/Al molar ratio = 50, 30 and 10) were synthesized *via* a surfactant templated approach by using fumed silica and aluminum sulfate as Si and Al precursors, respectively. When the 12-tungstophosphoric acid was grafted onto the surface of WSA*n*, a high dispersion of the heteropolyacid was achieved on the heteropoly compound/WSA*n* hybrid catalysts. The *Keggin* structure of the dispersed 12-tungstophosphoric acid was primarily preserved without destruction, but it was distorted in some degree, as confirmed by FTIR, ^{31}P NMR-MAS and UV–vis spectroscopic characterizations. The surface Brönsted acidity of the catalysts was greatly enhanced by several times in comparison to that of the bare WSA*n* support. In the hydroisomerization reaction of n-heptane, the Pt/$H_3PW_{12}O_{40}$/WSA30 catalyst exhibited the highest catalytic activity and the best isomerization selectivity among the catalysts tested, which can be generally correlated with its large number of Brönsted acid sites and high structural regularity. After the n-heptane hydroisomerization reaction, a high molar ratio of multibranched to monobranched isohexanes was obtained, indicating that Pt-promoted heteropoly compound/WSA*n* hybrid catalysts have a great potential for the hydroisomerization of long carbon chain hydrocarbons.

1. Introduction

Heteropolyacids have been widely investigated as catalysts in many acid-catalyzed and oxidation reactions due to their strong acidity, high oxidation potential and redox character [1–4]. These heterocompounds are usually composed of the primary, secondary and tertiary units. The primary unit is the most common and thermally stable structure, which is called as *Keggin* structure, it consists of a central atom (usually P, Si, or Ge) in the tetrahedral arrangement of oxygen atoms, surrounded by 12 oxygen octahedra containing the addenda atoms. The oxygen atoms in the *Keggin* unit can be classed into central oxygen atoms, two types of bridging oxygen atoms and terminal oxygen atoms [5].

In the catalysis application, the disadvantages of pure heteropolyacids used as catalysts are their very low surface area (<5 m^2/g) and nonporosity. Therefore, in order to make the most of their properties, it is necessary to disperse them onto a support with a large surface area and a proper pore system. Ordered mesoporous materials have been considered a suitable support for dispersing the heteropolyacids because of their large surface area, big pore diameter and great pore volume. In our previous papers, zirconium-modified MCM-41 mesoporous solids were used as heteropolyacid support, finding tungstophosphoric acid-grafted Pt/Zr-MCM-41 catalysts very active for the isomerization of hydrocarbons, like n-hexane and n-heptane, in the presence of hydrogen [6–8].

The Al-MCM-41 mesoporous solid is another candidate as heteropolyacid catalyst support. Since Al-MCM-41 materials possess surface acidity, when the heteropolyacid is loaded onto its surface, the interaction between the heteropolyacid and the support is not as strong as if dispersed on a base-character support, thus the possible surface acid–base reaction might be avoided, and the *Keggin* unit of the heteropolyacid, source of the strong Brönsted acidity, can be preserved. The Al-MCM-41 can be synthesized through several approaches, by varying the synthesis conditions, using different Al and Si precursors and different templates [9–11]. In the present work, in order to reduce the cost of Al-MCM-41 materials, we tried to use fumed silica and $Al_2(SO_4)_3$ as Si and Al source. In the catalysts preparation procedure, H_2PtCl_6 was the precursor of the metallic Pt active

* Corresponding author. Tel.: +52 55 57296000x55392; fax: +52 55 55862728.
E-mail address: chenglf2001@yahoo.com (L.F. Chen).

0920-5861/$ – see front matter © 2009 Elsevier B.V. All rights reserved.
doi:10.1016/j.cattod.2009.03.022

component and 12-tungstophosphoric acid was selected as acid promoter because this heteropolyacid has the *Keggin* structure with the stronger acidity and higher thermal stability, in comparison with other heteropoly compounds. In Pt-promoted heteropoly compound/Al-MCM-41 hybrid catalysts, the *Keggin* structure of the dispersed heteropolyacid is a key factor related to the catalytic properties. Therefore, the *Keggin* structure of the dispersed heteropolyacid was investigated by a variety of spectroscopic techniques like FTIR, ^{31}P NMR-MAS and UV–vis. The morphology of the Pt/HPW/Al-MCM-41 was observed by the TEM method and the surface acidity was measured by means of the FTIR of pyridine adsorption method. The catalytic activity and selectivity were evaluated in the hydroisomerization reaction of n-heptane under atmospheric condition.

2. Experimental

2.1. Catalyst support and catalysts preparation

2.1.1. Al-MCM-41 synthesis

Three Al-MCM-41 samples were prepared using $Al_2(SO_4)_3$ as aluminum source and cetyltrimethylammonium bromide (CTAB) as synthesis template. A typical preparation procedure of an Al-MCM-41 sample with a Si/Al = 50 molar ratio is described as follows: first of all, three solutions were prepared, the first solution was prepared by combining 10.1 ml of tetrabutylammonium hydroxide (TBAOH, 40% solution in water) with 4.31 ml of sodium silicate dispersed in 50 ml of water with stirring. The second one was prepared by adding 18.2 g of CTAB into 150 ml of hot water (50 °C) with agitation, and the last one was prepared by dissolving 1.4 g of $Al_2(SO_4)_3$ into 50 ml of water. Afterwards, the first solution was added into the second one and stirred for 30 min, followed by the addition of 4.52 g of fumed SiO_2 into this mixture with vigorous agitation for 2 h to form a gel. Then the third solution was added, drop by drop, into the above gel and further stirred for 1 h. The pH value of the gel was maintained at 11 by adding diluted sulfuric acid (0.2 M) during the agitation. The mixture was transferred into a Teflon bottle and heated to 80 °C for 72 h. The resultant white solid was filtered and washed extensively with 500 ml of deionized water for four times, and then dried in air at 80 °C for 24 h. Finally, the resultant solid was calcined at 600 °C for 6 h in air with a flow rate of 60 ml/min. The Si/Al molar ratio of the resultant solid is 50. The other samples with Si/Al = 30 and 10 molar ratios were prepared by a similar procedure. Hereafter the samples prepared with this method are denoted as WSA*n* (*n* = 50, 30, 10).

2.1.2. Catalysts preparation

A typical preparation procedure of the Pt/HPW/WSA*n* catalyst is described as follows: first, a calculated amount of $H_3PW_{12}O_{40}$ (HPW) was dissolved into given amounts of methanol (99.9%), the volume of methanol is controlled to a ratio of 10 ml methanol per gram of support. Afterwards, a calculated amount of Al-MCM-41 mesoporous materials was added into the $H_3PW_{12}O_{40}$–methanol solution to obtain a suspension mixture, this mixture was transferred into a rotary evaporator which was placed in a water bath at a 40 °C temperature. After the complete evaporation of methanol, the dry solid, showing a slightly yellow colour, contains 25 wt.% of $H_3PW_{12}O_{40}$. The 25 wt.% $H_3PW_{12}O_{40}$/Al-MCM-41 sample was dried at 80 °C for 24 h and calcined at 350 °C for 2 h. The 25 wt.% $H_3PW_{12}O_{40}$/Al-MCM-41 solid was then impregnated with the H_2PtCl_6 water solution. The Pt impregnation process was the same as the previously described. Finally, the 1 wt.%Pt/25 wt.%$H_3PW_{12}O_{40}$/Al-MCM-41 catalysts were obtained. Hereafter, the catalysts are denoted as Pt/HPW/WSA*n*.

2.2. Surface characterization of Al-MCM-41 and Pt/HPW/WSAn catalysts

2.2.1. Measurement of N_2 adsorption–desorption isotherms

The specific surface area, pore volume and pore size distribution of the samples were measured with a Digisorb 2600 equipment by low temperature N_2 adsorption–desorption isotherms. Before the measurement, the sample was evacuated at 350 °C. The surface area was computed from these isotherms by using the multi-point Brunauer–Emmett–Teller (BET) method based on the adsorption data in the partial pressure P/P_o range from 0.01 to 0.2. The value of 0.1620 nm^2 was taken for the cross-section of the physically adsorbed N_2 molecule. The mesopore volume was determined from the N_2 adsorbed at a P/P_o = 0.4. The pore diameter and pore volume were determined by using the BJH method. In all cases, correlation coefficients above 0.999 were obtained.

2.2.2. Magic angle spinning nuclear magnetic resonance (MAS-NMR)

Solid-state ^{31}P MAS-NMR spectra were recorded on a Bruker 400 MHz spectrometer at room temperature at a frequency of 79.49 MHz. A magic angle spinning rate of 7.5 kHz was employed, sending pulses at 90 s intervals and employing 4 mm zirconia rotors. The number of accumulations was 500. All the measurements were carried out at room temperature under Ar atmosphere for direct quantification. In order to protect the solid samples from moisture, the samples were stored inside a vacuum oven before and after measurements. Air was used as driving gas in order to obtain as much benefit as possible from the O_2 paramagnetic relaxation. The accuracy of the chemical shift determination was within ±0.1 ppm. For ^{31}P analysis, 85% H_3PO_4 solution (0 ppm) was used as standard reference, for measuring the chemical shift. The spectral deconvolution was performed with the Unity spectrometer software in an unconstrained manner.

2.2.3. High resolution transmission electron microscopy (TEM)

High resolution electron microscopy images of the mesoporous materials and catalysts were carried out with a JEOL 4000 EX electron microscope equipped with a pole piece with a spherical aberration coefficient of C_s = 1.00 mm. The powder samples were grounded softly in an agate mortar and dispersed in isopropyl alcohol in an ultrasonic bath for several minutes. A few drops were then deposited on 200 mesh copper grids covered with a holey carbon film. The electron micrographs were recorded in electron negative films and in a digital PC system attached to the electron microscope. The particle size distribution was evaluated from several micrographs taken from the same sample.

2.2.4. Ultraviolet–visible spectroscopic analysis (UV–vis)

The UV–vis diffuse reflectance spectra of the samples were collected on a Varian Cary 1G UV–visible spectrometer at room temperature. All the catalysts used for UV–vis analysis were calcined at 350 °C. Scan control conditions: average time 0.10 s; data interval 1.00 nm; scan rate 600 nm/min; mode: absorption; wavelength range: 190–900 nm.

2.2.5. FTIR spectroscopy of pyridine adsorption

To evaluate and analyze the strength and type of the acid sites, pyridine adsorption on the solid samples was performed on a 170-SX Fourier-transform infrared (FTIR) spectrometer in the temperature range between 25 and 400 °C. Before pyridine adsorption, the samples were heated to 400 °C under vacuum, and then cooled to room temperature. Afterwards, the solid wafer was exposed to pyridine, by breaking inside the spectrometer cell, a capillary containing 50 μl of liquid pyridine. The IR spectra were recorded at various conditions by increasing the cell temperature from 25 to 400 °C.

The quantitative calculation of Lewis acid sites and Brönsted acid sites was made with respect to the integrated area of the adsorption band at approximately 1450 and 1540 cm^{-1}, respectively. Integrated absorbance of each band is obtained using the appropriate software and the acid sites number calculation has been established by several authors with the corresponding extinction coefficient and the weight of the sample [12,13]. The acid strength was determined with respect to the variation of the number of acid sites as a function of the temperature.

2.3. Catalytic evaluation

The catalytic reactions for n-heptane isomerization were carried out in a down-flow fixed-bed U-shape reactor (i.d. = 1 cm, 20 cm in length) in the presence of hydrogen at atmospheric condition. The catalyst loading was 0.2 g and the H_2/n-heptane molar ratio was 12. The liquid n-heptane was placed inside a glass saturator in a water bath; the partial pressure of the n-heptane stream could be controlled by adjusting the temperature of the water bath. Hydrogen (99.9%) was passed through the saturator carrying the n-heptane stream into the reactor at a 40 ml/min flow rate. In the present experiment, the partial pressure of n-heptane was 0.077 atm. The reaction temperature was varied from 200 to 440 °C with a programmed temperature control system at a heating rate of 5 °C/min. The weight hourly space velocity (WHSV) was 3.78 h^{-1}. Before the reaction, the catalysts were reduced at 350 °C for 2 h using hydrogen in order to reduce the platinum oxide to metallic Pt.

The products distribution was analyzed using an on-line analytical system (GC Varian3300) equipped with a flame ionization detector (FID) and a HP-PONA 50 m × 0.2 mm capillary column which was maintained at 30 °C. The temperature of the FID detector was 300 °C. The catalytic activity was expressed as n-heptane conversion (%).

After 5 min at a setting temperature, we started to record the experimental data. The catalytic conversion and selectivity reported in the present work were the average of triple measurements at a reaction temperature. Each measurement took approximately 11 min. Therefore, to obtain an average catalytic activity at a given reaction temperature, around 38–40 min were used. The n-heptane isomerization reaction was carried out in the conditions where no external or internal diffusion limitation impeded the catalytic measurements. The yield of the product i (y_i) was defined as the mole fraction of the corresponding product relative to that all of the products, which can be calculated according to the formula: $y_i = S_i \times C_{heptane}$.

3. Results and discussion

3.1. FTIR characterization of Al-MCM-41

The surface features of the Al-MCM-41 support are related to external hydroxyl groups and retained surfactant template, which have great influence on the dispersion of the heteropolyacid. *In situ* FTIR spectroscopy studies allowed to analyze the changes of the surface properties and the surfactant incorporation into and removal from the Al-MCM-41 solid. The FTIR *in situ* spectra of the as-prepared WSA*n* (n = Si/Al = 50, 30, 10) samples calcined at various temperatures inside the IR cell are very similar; herein we only present a set of FTIR spectra of the WSA-30, as example. The IR spectra of the WSA30 sample recorded at 25 °C in Fig. 1, show a very broad absorption band covering the region between 3700 and 3000 cm^{-1}, corresponding to hydrogen-bonded hydroxyls and to water adsorbed on the sample surface. Two IR bands are observed between 3000 and 2850 cm^{-1}, characteristic of the C–H bond stretching vibrations

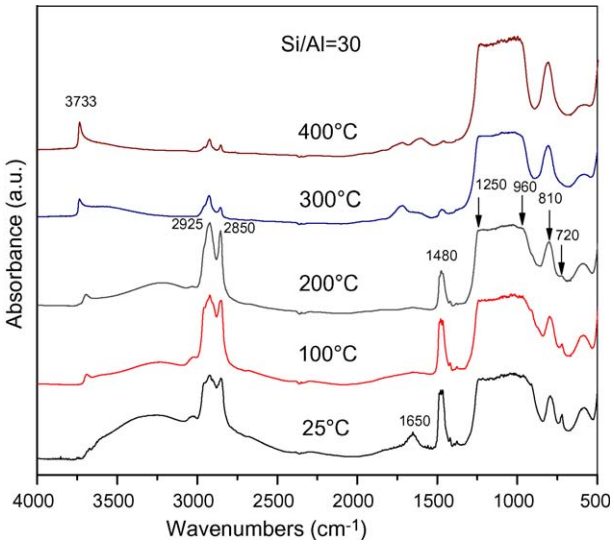

Fig. 1. A set of *in situ* FTIR spectra of the WSA30 sample.

in hydrocarbons, belong to the surfactant [14,15]. There is an intense band located at 1650 cm^{-1}, assigned to the flexion vibration of the OH bond. In the C–C stretching and C–H deformation vibrations region, the band located at approximately 1480 cm^{-1}, could be produced by bending mode vibrations (scissoring and rocking vibrations) of the C–H bond, of the $-CH_2-$ and $-CH_3$ groups in the surfactant. In addition, the rocking vibration of the C–H bond in the $N-CH_3$ surfactant head group was observed at around 720 cm^{-1} [14,15]. These observations confirm that the surfactant cations strongly interacted with the solid network during the preparation, and that they were not completely removed during the washing step.

The FTIR spectra also show several absorption bands below 1300 cm^{-1}, some peaks, like the wide peak between 1260 and 950 cm^{-1} and the one at 810 cm^{-1} are mostly due to fundamental antisymmetric and symmetric vibrations of the ≡Si–O–T (T = Si or Al) and ≡Si–O–Si≡ framework linkages. Because both, the $Si-O^-$ and the $Al-O^-$ stretching bands appear very close within the same region, they cannot be clearly distinguished. However, a small shift towards a higher wavenumber can be noticed for the Al-MCM-41 if compared to the siliceous Si-MCM-41, as a result of the incorporation of Al for Si in the framework structure. All these features are characteristic of the aluminosilicate MCM-41 structure.

When the IR cell temperature was increased to 100 °C, the intensity of the wide band between 3700 and 3000 cm^{-1} remarkably decreased and a weak band at around 3700 cm^{-1} appeared. This band is assigned to the M–OH (M = Al or Si) stretching frequency; while, several bands at 3070, 2980, 2925 and 2850 cm^{-1} were observed. The small band at 3070 cm^{-1}, is probably due to the stretching mode of CH_3 groups linked to the $-N(CH_3)_3+$ polar heads of the surfactant [16,17]. The three bands at 2980, 2925 and 2850 cm^{-1} correspond to C–H stretching bonds (νCH_{3as}, νCH_{2as} and $\nu(CH_{2as} + \nu CH_{3as})$) [15–18]. These bands seem to become sharper in comparison with the ones at 25 °C, however, when the covering effect produced by the broad peak of the adsorbed water at 25 °C is taken into account, they almost remained unchanged at 100 °C. The band at 1480 cm^{-1}, related to bending mode vibrations of the C–H bonds also remained unchanged. However, the one at 1650 cm^{-1} disappeared, in good agreement with the strong decreasing in intensity of the wide band between 3500 and 3700 cm^{-1}. These results indicate that most of the adsorbed water is desorbed at 100 °C; however, the incorporated surfactant has not been removed yet. The IR

Table 1
IR absorption bands assigned to particular vibration frequencies.

Absorption bands (cm^{-1})	Assignments	Refs.
3738–3740	Isolated Si–OH stretching mode	[13,14]
3690–3700	Hydrogen-bonded Si–OH stretching mode	[13,14]
3025–3040	CH_3 groups in $-N(CH_3)_3+$ stretching mode Polar heads of the surfactant	[15,16]
2960–2950	CH_3 groups in hydrogen–carbon chain, νCH_{3as}	[13–17]
2850–2855	CH_2 groups in hydrogen–carbon chain, νCH_{2as}	[13–17]
1750–1740	C–O bond in coke-like species	[13]
1600–1650	Flexion vibration of the –OH group in H_2O	[13]
1450–1500	Bending modes of C–H bonds in CH_3 or CH_2 groups scissoring and rocking vibrations, δCH_{3as} δCH_{2as}	[13–17]
1200–950	Si–O–Si and Si–O–Al vibrations	[15]
790–800	C–H rocking vibration Si–CH_3 streching mode	[15]
720	Rocking vibration of the C–H bond in the N–CH_3	[13,14]

absorption bands assigned to particular vibration frequencies are summarized in Table 1.

When the temperature gained up to 200 °C, as the adsorbed water further desorbed, the bands at around 3700 cm^{-1}, and those at 2800–3000 cm^{-1} became sharper. At 300 °C, the band at 1480 cm^{-1} was remarkably reduced in intensity. At 400 °C, the group bands at 2800–3000 cm^{-1} were strongly reduced and the one at 1480 cm^{-1} disappeared; instead, the one at 3700 cm^{-1} shift to 3750 cm^{-1} and became sharper. Several bands between 1800 and 1400 cm^{-1} appeared. These might have originated from the trace carbonate-like species resulting from the surfactant decomposition [14]. The *in situ* IR characterization of the samples could not be carried out at temperatures above 400 °C, however, the normal IR spectroscopy characterization of the solid showed that surface trace carbonate-like species can be removed by calcination at 600 °C. The solids calcined at 600 °C show M–OH groups on the surface, which is important, because they can associate with heteropolyacid compounds, thus inducing a high dispersion of them on the surface.

3.2. Characterization of the Keggin structure of the catalysts

3.2.1. FTIR characterization

For the characterization of the *Keggin* structure of the Pt-promoted heteropolyacid/Al-MCM-41 hybrid catalysts, it is useful to compare IR results with those of the pure $H_3PW_{12}O_{40}$. Usually, several IR bands at 1080, 982, 893, 799, 595 and 525 cm^{-1} can be observed for the unsupported $H_3PW_{12}O_{40}$. These intense bands arising from 1100 to 650 cm^{-1} can serve as signature of the *Keggin* anion [19,20]. The P–O symmetric stretching is characterized by the vibrational transition at 1080 cm^{-1}. The bands at 893 and 799 cm^{-1} are associated with the stretching motion of W–O–W bridges. The normal mode related to the band at 982 cm^{-1} is defined predominately by the W=O_d stretching mode. The band at 893 cm^{-1} may be described as a W–O_b–W stretching mode (inter-bridges between corner-sharing octahedral) and the band at 799 cm^{-1} is attributed to W–O_c–W stretching mode (intra-bridges between edge-sharing octahedral).

The IR features of the three catalysts are very similar. Fig. 2 shows the IR absorption domain for the *Keggin* units of the Pt/$H_3PW_{12}O_{40}$/WSA30 catalyst subtracted from IR absorption of the WSA30 matrix, in order to eliminate the absorption effect of the support. It is clear that the four fingerprint absorption bands corresponding to the heteropolyanion vibrations are similar to those of the pure $H_3PW_{12}O_{40}$, although the position of the absorption bands has small blue shifts [19,20]. The band at 1087 cm^{-1} does not split into two components, at 1085 and

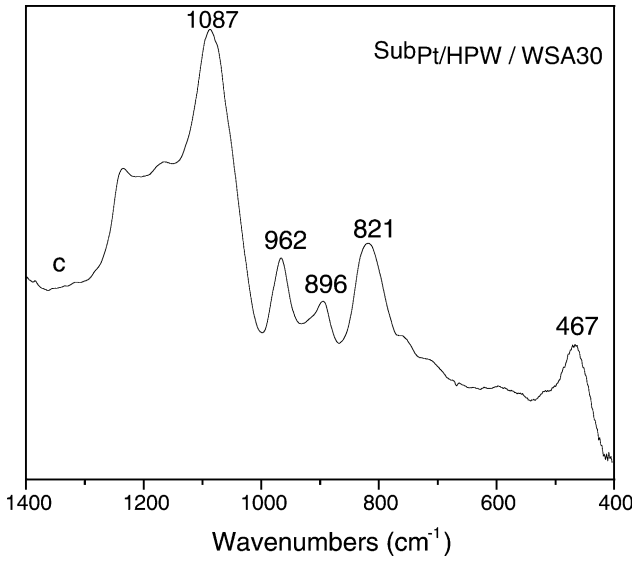

Fig. 2. A FTIR spectrum of the Pt/$H_3PW_{12}O_{40}$/WSA30 substracted from that of the WSA30.

1040 cm^{-1}, that usually indicates the formation of $[PW_{11}O_{39}]^{7-}$ [21]. According to IR spectroscopic findings, the heteropolyacid largely retains its primary structure after dispersion on the Al-MCM-41 support. However, the IR bands become broader with position shifts relative to that of the pure heteropolyacid, which may be explained by the interaction between the dispersed $H_3PW_{12}O_{40}$ and the support, this will be further characterized with additional techniques such as ^{31}P MAS-NMR and UV–vis spectroscopy.

3.2.2. UV–visible spectroscopic analysis

The UV spectra of the Pt/$H_3PW_{12}O_{40}$/WSA*n* catalysts are shown in Fig. 3. Two bands were observed at 204 and 253 nm, respectively. It has been reported that the pure HPW present $O^{2-} \rightarrow W^{6+}$ charge transfer absorption bands with maximum at approximately 255 and 350 nm [22]. With respect to the pure HPW, the UV band positions of the Pt/$H_3PW_{12}O_{40}$/WSA*n* catalysts were clearly shifted towards a lower wavelength range. Similar observations on HPW/Al_2O_3 and HPW/SiO_2 were also reported by other researchers [23]. These observations indicate that a very high dispersion of the heteropolyacid is attained on the Al-MCM-41 support or, that the *Keggin* structure is deformed due to the interaction between the heteropolyanions and the support.

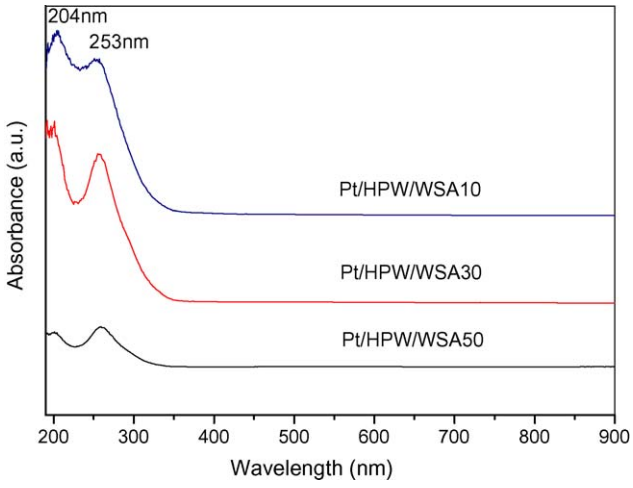

Fig. 3. UV–vis spectra of the Pt/HPW/WSA*n* catalysts.

It has been established the relationship between the energy transition involved in UV radiation absorption and the diameter of the nanoparticles, as expressed by Eq. (1):

$$\Delta E = \frac{h^2}{8R^2(1/m_e + 1/m_h)} \quad (1)$$

where ΔE is the energy change associated to the band gap, due to the quantum size effect, h is the Planck constant, R is the radius of the quantum dot, m_e is the effective mass of an electron and m_h is the effective mass of a hole. It is clear that the absorption energy of the quantum dot varies with the R-value. Therefore, for nanoparticles in the quantum dot range, the frequency of the absorbed UV light usually shifts towards a lower wavelength as the particle diameter decreases. The shift of the UV–vis bands positions of the $Pt/H_3PW_{12}O_{40}$/Al-MCM-41 relative to that of the pure HPW strongly indicates a smaller particle size, thus a high dispersion of the heteropolyacid on the Al-MCM-41 support.

3.2.3. ^{31}P MAS-NMR spectroscopic analysis

The stability of the *Keggin* structure of the catalysts after calcination was also investigated by the solid-state ^{31}P MAS-NMR technique. The ^{31}P MAS-NMR spectra of the 1 wt.%Pt/25 wt.%$H_3PW_{12}O_{40}$/WSA*n* catalysts are shown in Fig. 4. As we know that bulk HPW exhibits one sharp, intensive peak with a chemical shift at approximately $\delta = -15.00$ ppm, characteristic of the $[PW_{12}O_{40}]^{3-}$ anion with a *Keggin* structure [24,25]. Compared to pure HPW, the ^{31}P MAS-NMR spectra of the Pt/HPW/WSA*n* catalysts show a few differences:

(i) The peak position shifted towards the left direction.
(ii) The peak is notably wider.
(iii) The spectrum of the Pt/HPW/WSA50 sample consists of two signals: the main one at $\delta = -13.49$ and the small one at -15.66 ppm.

It has been reported that $H_3PW_{12}O_{40}$ supported on TiO_2 exhibits four peaks at -4, -8, -11 and -13 ppm, assigned to adsorbed phosphorus species deriving from a highly fragmented *Keggin* unit and a defective and deformed *Keggin* structure interacting with surface hydroxyl groups, respectively [26]. Therefore, the dispersed heteropolyanions with structures different from the pure HPW bulk crystal were formed on the $Pt/H_3PW_{12}O_{40}$/WSA*n* catalysts: the position shift and peak widening indicate the deformation of the *Keggin* unit and a high dispersion of the heteropolyacid. The peak at approximately -13.49 ppm probably resulted from a deformed $H_3PW_{12}O_{40}$ structure, due to interaction with surface hydroxyl groups of the support, which indicates that $H_3PW_{12}O_{40}$ clusters or small particles with distorted *Keggin* units exist on the surface of the Al-MCM-41 support in a high dispersion. For all of the three samples, no peaks around -11 or -8 ppm (generally attributed to defective or lacunary $(P_2W_{21}O_{71})^{6-}$ units) were evident; also no peak at -4 ppm was observed, indicating that no fragmented *Keggin* units were formed. For the small peak at approximately 15.56 ppm in the Pt/HPW/WSA50 catalyst, it seems to be related to the weak interaction between the support and the *Keggin* unit. This sample contains a small amount of hydroxyl groups on the surface, due to less aluminum content; therefore, a small amount of the heteropolyacid kept the *Keggin* units the same as in the bulk or pure heteropolyacid phase. One may see that although it was deformed in certain degree, the primary structure of the tungstophosphate heteropolyanions is largely preserved without destruction, after impregnation on the Al-MCM-41 mesoporous support.

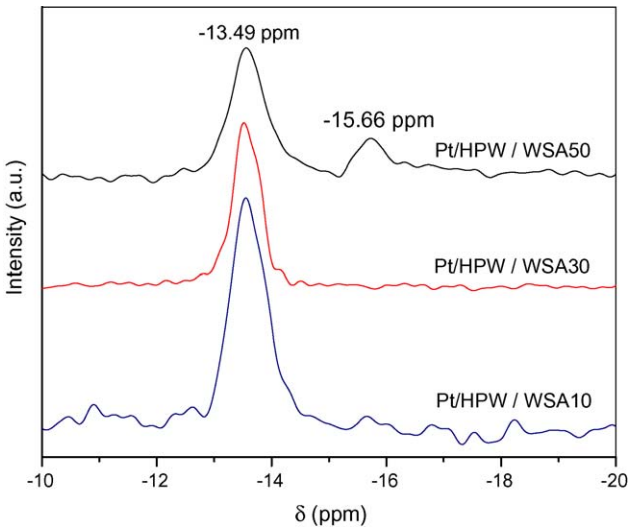

Fig. 4. ^{31}P MAS-NMR spectra of the Pt/HPW/WSA*n* catalysts.

3.3. Textural properties of the catalysts

The textural properties of the catalysts were measured by means of N_2 adsorption–desorption isotherms. The related data are reported in Table 2. In order to see the changes of the textural properties, the data of the bare WSA*n* samples are also comparatively shown in Table 2. The surface area is 609.1 and 625.1 m^2/g for the Pt/HPW/WSA50 and Pt/HPW/WSA30 catalysts, respectively. However, the surface area of the Pt/HPW/WSA10 catalyst is remarkably reduced to 201.8 m^2/g. This is because the surface area of the WSA10 support is only 215.7 m^2/g; while its pore diameter is 18.1 Å, which are three times greater than that the other two samples, indicating that the pore system of the WSA10 sample has partially collapsed. These results show that too high aluminum content in the Al-MCM-41 sample is unfavourable to the formation of the ordered mesoporous solid. The average pore diameter of the Pt/HPW/WSA50 and Pt/HPW/WSA30 catalysts lies between 6.0 and 7.0 nm. There are two kinds of pores with different pore diameter formed in these solids. Most of the pores have an approximately 2–3 nm diameter and a small part of the pores have a large size due to the collapsing of the pore wall during the calcination.

3.4. Morphological features of the catalysts

The dispersion, location and size of the heteropolyacid species of the Pt/HPW/Al-MCM-41 catalysts were also investigated by high resolution TEM (Fig. 5). Fig. 5a clearly shows that most of the heteropolyacid is uniformly distributed on the surface of the support. As shown in the enlarged image (Fig. 5b), the pores with 2.5–3 nm diameter can be clearly seen but their openings are covered with web-network-like materials. However, these pores are not completely blocked. These observations confirm that the

Table 2
Textural data of the WSA*n* and Pt/HPW/WSA*n* catalysts.

Si/Al ratio		Surface area (m^2/g)		Average pore diameter (nm)		Pore volume (cm^3/g)	
n[a]	*r*	WSA*n*	Pt/HPW/WSA*n*	WSA*n*	Pt/HPW/WSA*n*	WSA*n*	Pt/HPW/WSA*n*
50	46.1	620.1	609.4	5.1	6.7	0.97	1.018
30	30.8	780.0	625.1	4.2	6.0	1.04	0.985
10	8.3	215.7	201.8	18.8	15.4	1.13	0.773

[a] *n*, nominal; *r*, real.

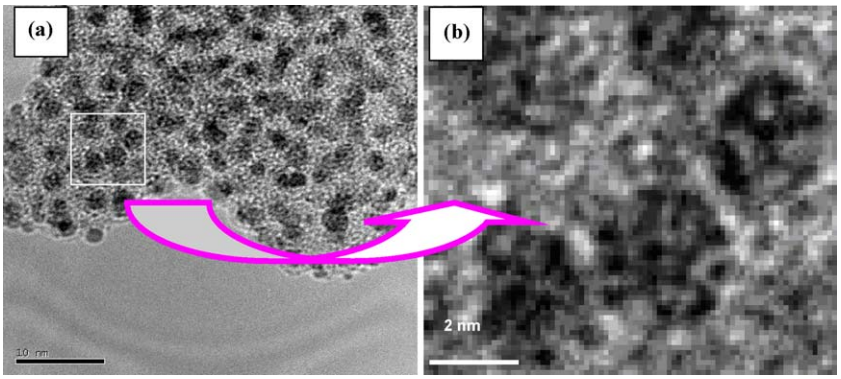

Fig. 5. TEM images of the Pt/HPW/WSA*n* catalyst. (a) Pt/HPW/WSA30; (b) close observation of marked area in image.

dispersion of the heteropolyacid is homogeneous and uniform, no large heteropolyacid particles or aggregates were formed.

The molecular diameter of the $H_3PW_{12}O_{40}$ molecule is estimated to be 1–1.2 nm, which is smaller than the average dimension of the pores (6–7 nm). Therefore, it is possible that the HPW locates inside the internal pore wall of the support. However, it is also possible that the HPW molecules may also form nanoclusters by assembling several molecules, thus particle diameter larger than the dimension of the most ordered pores; therefore, the heteropolyacid may locate inside the internal pores, or may be dispersed on the external surface of the support.

3.5. Surface acidity of the Pt/HPW/WSAn catalysts

The surface acidity of the 1 wt.%Pt/25 wt.%$H_3PW_{12}O_{40}$/WSA*n* catalysts was measured by the *in situ* FTIR spectroscopy of pyridine adsorption technique (Figs. 6–8). Usually, the bands at approximately 1450 and 1620 cm^{-1} are assigned to Lewis acid sites; while the bands at around 1540 and 1635 cm^{-1} are indicative of the existence of Brönsted acid sites [27,28]. On the basis of the aforementioned assignments of the IR absorption bands, it can be confirmed that both, Lewis and Brönsted acid sites, coexist on all the three catalysts. The catalyst with WSA30 as support exhibits the largest number of Brönsted acid sites together with the highest acid density, among the three catalysts. It seems to indicate that the Brönsted acidity correlates with the population of Al aluminum ions in tetrahedral environments or aluminum ions in both positions with pentahedral and tetrahedral coordination because the WSA30 sample contains the biggest fraction of the Al ions with pentahedral and tetrahedral coordination.

When compared with the parent WSA*n* support, the number of Brönsted acid sites on the Pt/HPW/WSA*n* catalysts increased by approximately four times. The related acidity data are reported in Table 3. However, the number of Lewis acid sites diminished after heteropolyacid impregnation. As a result, the number of the total acid sites decreased. Blockage of Lewis acid sites due to deposition of the heteropolyacid might be responsible for the reduction of the Lewis acidity.

3.6. Catalytic properties

Fig. 9 shows the n-heptane conversion obtained with the Pt/HPW/WSA*n* catalysts at different temperatures. The most active catalyst corresponds to the Si/Al molar ratio = 30 support. Over the Pt/HPW/WSA30 catalyst, the n-heptane conversion is much higher than that over the other two catalysts.

The isomerization selectivity of the Pt/HPW/WSA*n* catalysts at different reaction temperatures is shown in Fig. 10. The highest selectivity to C_7 isomers is also achieved on the Pt/HPW/WSA30 catalyst. Thus, among the three catalysts tested, the Pt/HPW/WSA30 catalyst shows the best catalytic activity and isomerization selectivity in the n-heptane isomerization reaction, while the Pt/HPW/WSA10 catalyst exhibits the lowest catalytic activity and isomerization selectivity.

Several physicochemical properties may be related to the catalytic behaviours of the catalysts. First, it is noteworthy that, the

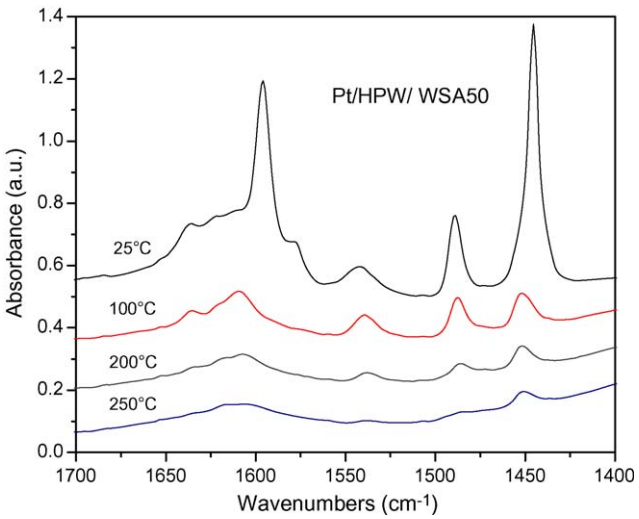

Fig. 6. FTIR spectra of pyridine adsorption on the Pt/HPW/WSA50 catalyst.

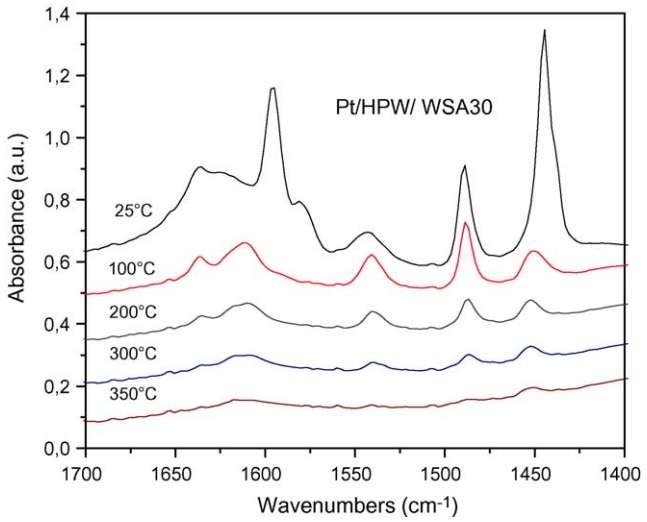

Fig. 7. FTIR spectra of pyridine adsorption on the Pt/HPW/WSA30 catalyst.

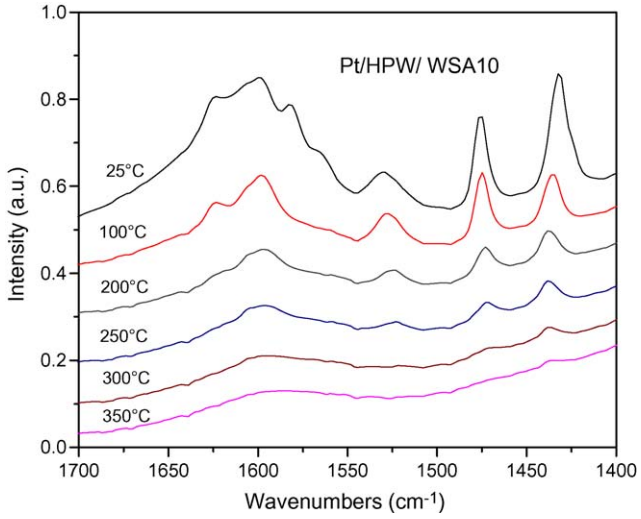

Fig. 8. FTIR spectra of pyridine adsorption on the Pt/HPW/WSA10 catalyst.

Table 3
Acidity results for the WSA*n* and $Pt/H_3PW_{12}O_{40}$/WSA*n* catalysts.

Samples	Brönsted acid sites (μmol/g)	Lewis acid sites (μmol/g)	Total acid sites (μmol/g)
WSA50	28	881	909
WSA30	50	1545	1595
WSA10	35	561	595
Pt/HPW/WSA50	115	722	837
Pt/HPW/WSA30	207	943	1150
Pt/HPW/WSA10	147	577	624

structural ordering of the WSA30 support is the best among the WSA*n* samples, which highly favours the diffusion of the reactants inwards the active sites and is beneficial for the outwards diffusion of branched isomers formed inside the channels. On the contrary, due to thermal instability at high aluminum content, the structure of the WSA10 solid is rather disordered after calcination and its pore system almost collapsed. Also the surface area of the Pt/HPW/WSA10 catalyst is much lower compared to other two catalysts. Second, the WSA30 support possesses a high content of Al ions in tetrahedral positions, as confirmed by ^{27}Al MAS-NMR analysis (70.1% Al ions occupy the tetrahedral positions); whereas, the WSA10 support contains many extra-framework Al ions (74.5% Al ions occupy octahedral positions). The extra-framework Al ions may catalyze cracking reactions, reducing the isomerization

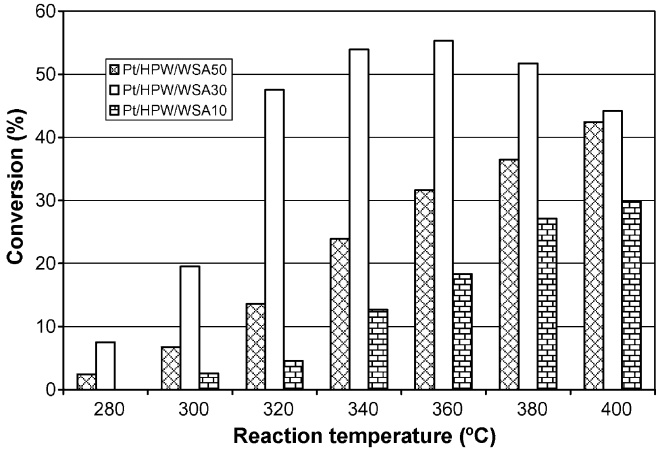

Fig. 9. Comparison of the n-heptane conversion by the Pt/HPW/WSA*n* catalysts.

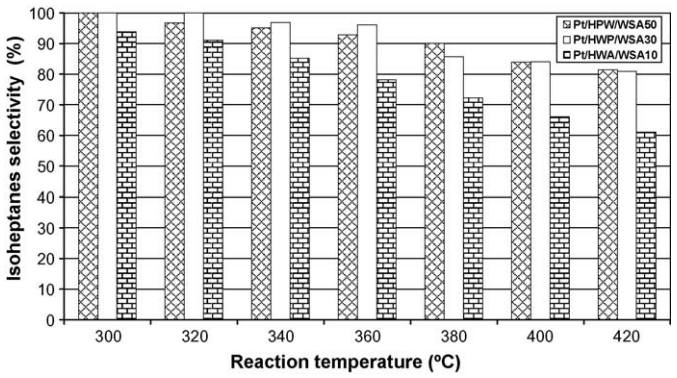

Fig. 10. Comparison of the selectivity of isoheptane for the Pt/HPW/WSA*n* catalysts.

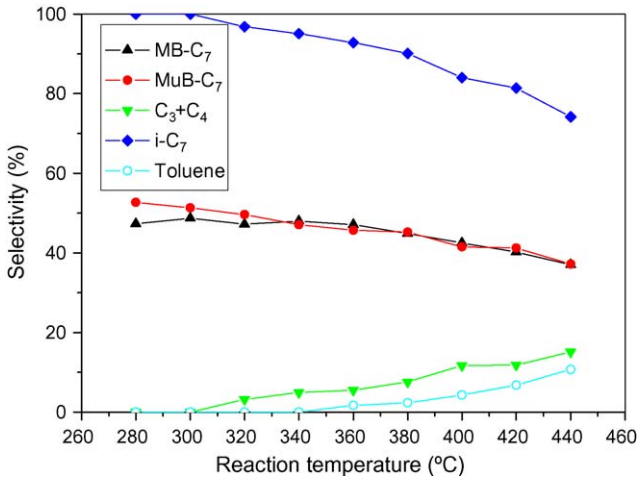

Fig. 11. Selectivity of various products over the Pt/HPW/WSA50 catalyst.

selectivity. Moreover, the Pt/HPW/WSA30 catalyst presents the highest number of Brönsted acid sites, compared to the other two catalysts. Based on these observations, it is believed that the selectivity of C_7 isomers over the Pt/HPW/WSA*n* catalysts is controlled by the surface acidity, aluminum ions cordinations as well as the structural regularity of the catalyst.

The selectivities of the different products obtained from the Pt/HPW/WSA*n* catalysts are shown in Figs. 11–13. Very similar to the products distribution obtained from the Pt/HPW/Zr-MCM-41 catalysts [6]: 2-methylhexane, 3-methylhexane, 2,2-dimethylpentane, 2,3-dimethylpentane, 2,4-dimethylpentane, 3,3-dimethyl-

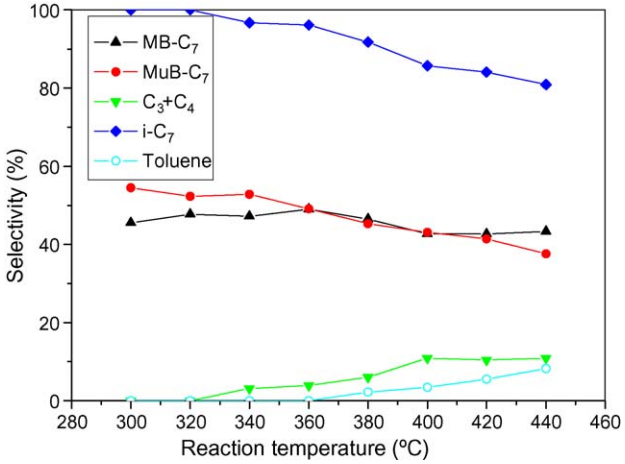

Fig. 12. Selectivity of various products over the Pt/HPW/WSA30 catalyst.

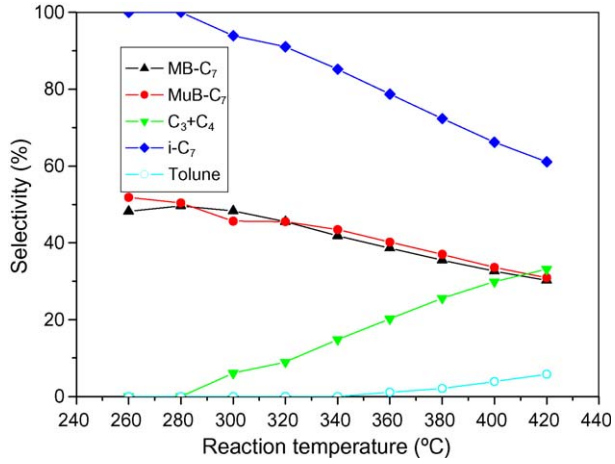

Fig. 13. Selectivity of various products over the Pt/HPW/WSA10 catalyst.

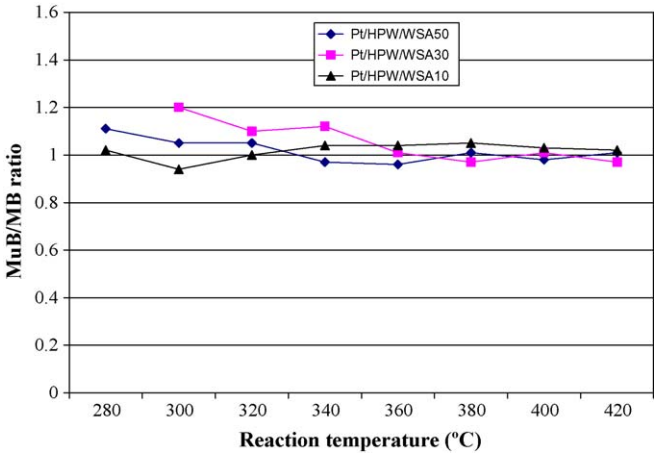

Fig. 14. Ratio of multibranched to monobranched isoheptanes of the Pt/HPW/WSA*n* catalysts as a function of the reaction temperature.

pentane and traces of 2,2,3-trimethylbutane are the isomer products. In the monobranched isomers, 2-methylhexane is predominant; and in the multibranched isomers, 2,3-dimethylpentane is the major component.

The ratio of multibranched to monobranched isomer products (R) as a function of the reaction temperature is plotted in Fig. 14. At each temperature or conversion level, the R-value is near 1 for all the Pt/HPW/WSA*n* catalysts. This result indicates that the ratio of monobranched to multibranched isomers is independent of conversion. From this result, the formation of the cracking products seem to be produced by the decomposition of both, monobranched and multibranched isomers, at high temperatures, as indicated by the simultaneous decrease of the selectivity of both, monobranched or multibranched isomers at a similar rate.

It is noted that for the Pt/HPW/WSA*n* catalysts, at a reaction temperature higher than 360 °C, less than 3.6% of toluene were formed. The toluene formation may go through two plausible pathways that are illustrated in Fig. 15. First of all, in the initial stage of the mechanisms, n-heptane can be dissociatively adsorbed on the metal active clusters to form an alkene-like intermediate ($\sigma C_7^{=}$) which may be transformed to toluene *via* two routes: (i) A cyclisation–dehydrogenation pathway. The cyclisation reaction may take place by the 1, 6 ring closure of the C_7 surface intermediate to produce methylcyclohexane which can be successively dehydrogenated on the catalyst surface, and finally, toluene is produced. (ii) An isomerization–cyclisation–dehydrogenation pathway. Part of the 3- or 2-methylhexyl intermediates can be cyclised and followed by dehydrogenation to form toluene besides methylhexanes formation.

It is speculated that toluene formation requires a relatively longer residence time for the corresponding intermediates at the active centres than that required for C_7 isomers formation. If the channels or the textural structure of the catalysts are well ordered, the reactants or the products may rapidly reach or leave from the active sites, with a short residence time within the pores, that is unfavourable to the formation of toluene. This can explain the fact that no toluene was formed over the Pt/HPW/CSAn catalysts which have relatively ordered structures prepared by using tetraethylorthosilicate (TEOS) as Si precursor and aluminum tri-sec-butoxide (97 wt.%) as aluminum source [29] and that toluene was formed on the Pt/HPW/WSA*n* catalysts which show a rather disordered wormhole-like mesoporous system reported herein.

Over all of the catalysts, the yield to cracking products linearly increases with increasing the reaction temperature, following the same pattern as with the Pt/HPW/Zr-MCM-41 and Pt/HPW/CSA catalysts [6,29]. Only propane, isobutane and n-butane were detected as the cracking products. It is noteworthy that n-C_4 is produced above 340 °C on all the catalysts, while, i-C_4 appears when cracking reactions take place. The isobutane yield is usually higher than that of n-C_4. The cracking products distribution is also very similar to that obtained using Pt/HPW/Zr-MCM-41 catalysts, indicating a similar pathway for the cracking reactions. n-C_4 and n-C_3 are formed *via* 2,3-dimethylpentane cracking, while i-C_4 and n-C_3 result from 2,2-dimethylpentane and 2,4-dimethylpentane cracking. Our results indicate that 2,3-dimethylpentane is rather stable below 340 °C in comparison with 2,2-dimethylpentane and 2,4-dimethylpentane. More cracking products are formed over the Pt/HPW/WSA10 catalyst, which may be correlated with its

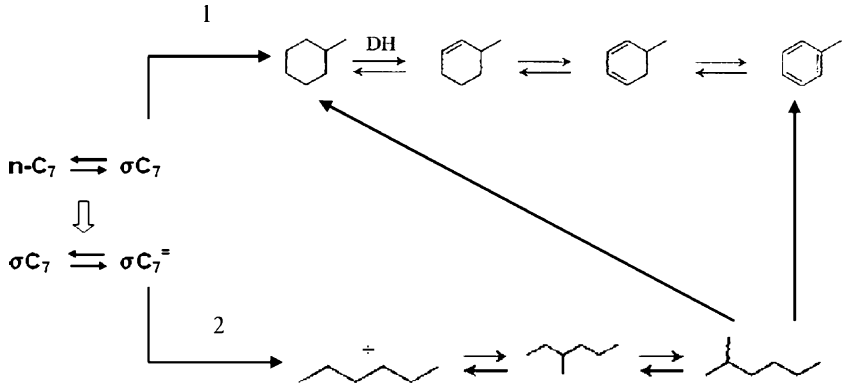

Fig. 15. Toluene formation mechanism.

disordered structure and poor textural properties as well as high fraction of aluminum ions at octahedral positions in the support.

4. Conclusions

Highly dispersed 12-tungstophosporic acid was grafted on the surface of the mesoporous Al-MCM-41, producing heteropoly compound/Al-MCM-41 hybrid catalysts containing a great number of Brönsted acid sites with strong acid strength. The *Keggin* units of the supported heteropolyacid were mostly preserved with certain degree of structural deformation after calcination. At atmospheric reaction conditions, a high yield of multibranched isoheptanes was produced in the n-heptane hydroisomerization reaction over the catalysts. The molar ratio of multibranched to monobranched isoheptanes is around 0.8–1.2, which is very close to its thermodynamic equilibrium value. This work shows that Pt-promoted heteropolyacid/Al-MCM-41 hybrid catalysts have a great potential for the hydroisomerization of long carbon-chain hydrocarbon applications.

Acknowledgments

L.F. Chen wishes to acknowledge the scholarship for her study of the doctorate degree offered by the CONACyT-Mexico. The financial support from the projects SIP-IPN (Nos. 20080745 and 20091076) and CONACyT (Mexico)-NSF (China) J110.243/2007. The authors thank Dr. A. Paz and Dr. I. Hernández for their help in the samples characterization.

References

[1] I.V. Kozhevnikov, Appl. Catal. A: Gen. 256 (2003) 3.
[2] K. Na, T. Okuhara, M. Misono, J. Mol. Catal. A: Chem. 115 (1997) 449.
[3] K. Na, T. Tkuhara, M. Misono, J. Catal. 170 (1997) 96.
[4] C. Travers, N. Essayem, M. Delage, S. Quelen, Catal. Today 65 (2001) 355.
[5] M.J. Janik, K.A. Campbell, B.B. Bardin, R.J. Davis, M. Neurock, Appl. Catal. A: Gen. 256 (2003) 51.
[6] J.A. Wang, L.F. Chen, L.E. Noreña, J. Navarrete, M.E. Llanos, J.L. Contreras, O. Novaro, Micropor. Mesopor. Mater. 112 (2008) 61.
[7] L.F. Chen, J.A. Wang, L.E. Noreña, J. Aguilar, J. Navarrete, P. Salas, J.A. Montoya, P. Del Ángel, J. Solid State Chem. 180 (2007) 2958.
[8] L.F. Chen, L.E. Noreña, J.A. Wang, X.L. Zhou, J. Navarrete, I. Hernández, A. Montoya, P. Pérez Romo, P. Salas, S. Castella Pergher, Catal. Today 133–135 (2008) 331.
[9] W. Zhang, M. Fröba, J. Wang, P.T. Tanev, J. Wong, T.J. Pinnavaia, J. Am. Chem. Soc. 118 (38) (1996) 9164.
[10] P. Wu, M. Iwamoto, J. Chem. Soc., Faraday Trans. 94 (1998) 2871.
[11] H. Kosslick, H. Landmesser, R. Frecke, J. Chem. Soc., Faraday Trans. 93 (9) (1997) 1849.
[12] C.A. Emeis, J. Catal. 141 (1993) 347.
[13] T. Barzzetti, E. Selli, D. Moscotti, L. Forni, J. Chem. Soc., Faraday Trans. 92 (1996) 1401.
[14] A. Laachir, V. Perichon, A. Badri, J. Lamotte, E. Catherine, J.C. Lavalley, J. El Fallah, L. Hilarer, F. Le Normand, E. Uenere, G.N. Sauvion, O. Touret, J. Chem. Soc., Faraday Trans. 87 (1991) 1601.
[15] A.V. Ivanov, E. Zausa, Y. Ben Taârit, N. Essayem, Appl. Catal. A: Gen. 256 (2003) 225.
[16] L.J. Bellamy, The Infra-red Spectra of Complex Molecules, Methuen, London, 1962.
[17] E. Gianotti, E.C. Oliveira, V. Dellarocca, S. Colucci, H.O. Pastore, L. Marchese, in: A. Sayari, M. Jaroniec (Eds.), Stud. Surf. Sci. Catal. 141 (2001) 471.
[18] V.B. Fenelonov, V.N. Romannikov, A.Y. Derevyankin, Micropor. Mesopor. Mater. 28 (1999) 1321.
[19] S. Choi, Y. Wang, Z. Nie, J. Liu, C.H.F. Peden, Catal. Today 55 (2000) 117.
[20] A.V. Ivanov, T.V. Vasina, V.D. Nissenbaum, L.M. Kustov, M.N. Timofeeva, J.I. Houzvicka, Appl. Catal. A: Gen. 259 (2004) 65.
[21] E. López-Salinas, J.G. Hernández-Cortéz, I. Schifter, E. Torres-García, J. Navarrete, A. Gutiérrez-Carrillo, T. López, P.P. Lottici, D. Bersani, Appl. Catal. A: Gen. 193 (2000) 215.
[22] L.R. Pizzio, C.V. Cáceres, M.N. Blanco, Appl. Catal. A: Gen. 167 (1998) 283.
[23] A. Rives, E. Payen, R. Hubaut, P. Vázquez, L. Pizzio, C. Cáceres, M. Blanco, Catal. Lett. 71 (2001) 193.
[24] A. Ghanbari-Siahkali, A. Philippou, J.M. Dwyer, W. Anderson, Appl. Catal. A: Gen. 192 (2000) 57.
[25] I.V. Kozhevnikov, K.R. Kloetstra, A. Sinnema, H.W. Zandbergen, H. van Bekkum, J. Mol. Catal. A: Chem. 114 (1996) 287.
[26] J.C. Wdwards, C.Y. Thiel, B. Benac, J.F. Knifton, Catal. Lett. 51 (1998) 77.
[27] T. López, J. Navarrete, R. Gómez, O. Novaro, F. Figueras, H. Armendáriz, Appl. Catal. A: Gen. 125 (1995) 217.
[28] D. Srinivas, R. Srivastava, P. Ratnasamy, Catal. Today 96 (2004) 127.
[29] J.A. Wang, L.F. Chen, L.E. Noreña, J. Navarrete, Appl. Catal. A: Gen. 357 (2009) 223.